http://dx.doi.org/10.5012/bkcs.2013.34.12.3547

Articles

Effect of VO(II) Doping on Structural and Optical Properties of Diaquamalonato(1,10-phenanthroline)zinc(II)

Ramesh Hema, Krishnan Parthipan,†,* Somasundaram Ramachitra,‡ and Subramanian Balaji

Department of Chemistry, SCSVMV University, Kanchipuram-631561, Tamilnadu, India
*†Depatment of Chemistry, A.M. Jain College, Meenambakkam, Chennai-600114. *E-mail: psr12in@gmail.com*
‡Department of Chemistry, Pondicherry University, Puducherry-605 014, India
Received July 11, 2013, Accepted September 3, 2013

Single crystal EPR and optical studies of a mixed ligand zinc(II) complex doped with VO(II) ion is carried out to establish the structural properties. The angular variation of vanadyl hyperfine lines indicates a single site, with spin Hamiltonian parameters as: g_{xx} = 1.985, g_{yy} = 1.979, g_{zz} = 1.943; A_{xx} = 8.71, A_{yy} = 6.41 and A_{zz} = 17.80 mT. By comparing the direction cosines of principal g and A values with the direction cosines of metal-ligand bonds, it has been confirmed that the vanadyl ion has entered the lattice interstitially. The exact interstitial position of VO(II) in host lattice has been calculated using the fractional coordinates of atoms in the host lattice out of many assumptions. The EPR and optical data have been confirmed to obtain various bonding parameters, from which the nature of the bonding in the complex is discussed. FT-IR confirms the formation of structure of host lattice.

Key Words : EPR, Vanadyl, Bonding parameters, Interstitial, Admixture coefficients

Introduction

Coordination polymers of malonic acid offered attractive properties such as metal organic frame work, supramolecular behaviors, biological properties, molecular electronics, catalysis and molecular based magnetic materials *etc.* Malonic acid is the most widespread dicarboxylic acid present in the natural vegetables predominantly in beetroot and legumes. It makes a prominent role in symbiotic nitrogen metabolism and also employs as competitive inhibitor of cellular respiration. Malonic acid with diethyl ester is used in the manufacture of vitamins B1, B6, barbiturates and numerous other valuable compounds, and also they are useful in biological and medicinal fields. As an example, malonate is a powerful competitive inhibitor for cellular respiration; because it binds with the active site of succinate dehydrogenase in the citric acid cycle.[1-4] Zinc complexes of malonic acid have number of dentating abilities. Malonic acid forms complexes of bridging types also. An important quality of Malonic Acid Bridge is that the magnitude of exchange interaction mainly depends on the bridging modes. Because of this, the malonate complexes exhibit ferro- or antiferro magnetic interactions, which are controlled by the dimensionality of the structure. Moreover, the carboxylate group affords an efficient pathway for the magnetic centers to couple either ferro or antiferromagnetically.[5-7] Zinc complexes with malonate ligand has found its importance in treating wounds and burns.[8] The probability of getting information about symmetry and geometry from magnetically concentrated systems is narrowed because of very broad resonance in EPR arising due to dipolar and exchange interactions. Hence, to study the symmetry around the embedded ion and covalence, paramagnetic ions should be incorporated into diamagnetic host lattices.[9,10] Transition metal ion doped crystals are useful for laser and optical fiber applications because of their spectroscopic behaviors. Vanadyl ion *i.e.*, VO(II), is used extensively in EPR studies to characterize phase transitions, strength and magnitude of crystal field relaxation times, *etc.*, as it is one of the most stable molecular paramagnetic transition metal ions having $t_{2g}^1e_g^0$ configuration. In addition, vanadium ion exists in bivalent, trivalent and tetravalent oxidation states. Out of these, VO(II) with a single unpaired 3d electron bound to an oxygen atom by a strong bond is well studied. The preferential orientation of the V=O bond in different complexes depends on the type of the ligands. Single crystal EPR studies reveal the location of paramagnetic impurity, *i.e.*, interstitial, substitutional or both and it tells about the symmetry of electric field around the paramagnetic ion in diamagnetic host lattices.[11-22] Past few years, our research has focused on single crystal EPR investigation of vanadyl doped zinc malonato complexes.[23-27] In this way, mixed ligands especially phenanthroline and malonic acid containing complex Diaquamalonato(1,10-phenanthroline) zinc(II) (here after abbreviated as DMPZ) has been selected as a host for doping of VO(II) ion by considering the applications of transition metal malonato complexes. Effects of dopant on structural properties, symmetry distortion and various bonding parameters of host

complex have been explored using single crystal EPR technique and optical absorption studies in the present work.

Experimental

Synthesis of VO(II)/DMPZ Single Crystals. Single crystal of VO(II)/DMPZ was grown by mixing equimolar mixture of aqueous solutions of zinc oxide and malonic acid for 1 h at 70 °C and an alcoholic solution of 1,10-phenanthroline was added with continuous stirring. To this, 0.2 mol % of $VOSO_4$ was added as dopant. After 30 mins, the reaction mixture was cooled to 300 K and it was filtered. Light blue colored vanadyl doped DMPZ crystals were obtained after couple of weeks. Anal. Calcd. (%) for VO(II)/DMPZ: C 46.92, H 3.67, N 7.30, Zn 13.62, V 2.65; Found (%) C 46.87, H 3.63, N 7.25, Zn 13.58, V 2.62.

Physical Measurements. The C, H, N microanalysis were carried out on elemental analyser and vanadium was estimated gravimetrically as its vanadate. The content of the zinc in VO(II)/DMPZ was determined by complexometric titration with EDTA. Optical absorption spectrum was recorded at 300 K using a Varian Cary 5000 Ultraviolet (UV–Visible) near infrared spectrophotometer in the range of 200-800 nm. FTIR spectra were recorded for doped and undoped materials on a Shimadzu FTIR-8300/8700 spectrometer in the range of 4000-400 cm^{-1}, using almost transparent KBr pellets containing fine powder sample. Powder XRD measurements were carried out for doped and undoped materials on a PANalytical X'pert PRO diffractometer with Cu Kα radiation of wavelength 0.15406 nm and 2θ values between 5° and 75°. EPR spectra were recorded at 300 K on a JEOL JESTE100 ESR spectrometer operating at X-band frequencies, having a 100 kHz field modulation to obtain first derivative spectrum. 1,1-Diphenyl-2-Picrylhydrazyl (DPPH) was used as standard for magnetic field correction. Angular variation plots were made by rotating the crystal along the three mutually orthogonal axes a, b, c* in 10° intervals. Isofrequency plots for each plane were simulated using program EPR–NMR. The EPR spectrum of powder sample was simulated using Simfonia program developed and supported by Brucker Biospin.

Crystal Structure. DMPZ ($[Zn(C_3H_2O_4)(C_{12}H_8N_2)(H_2O)_2]$) belongs to monoclinic crystal class with space group $P2_{1/C}$, having unit cell parameters, a = 1.034, b = 0.967, c = 1.548 nm, β = 105.72° and Z = 4. The zinc atom shows a distorted octahedral coordination sphere, coordinated by two N1 and N2 atoms from 1,10-phenanthroline, two O5 and O6 atoms from cis water molecules and two O1 and O3 atoms from malonic acid. The complex molecules are linked to form a three-dimensional supra molecular array by both hydrogen-bonding interactions between coordinated water molecules, uncoordinated carboxylate oxygen atoms of neighboring molecules and aromatic π-π stacking interactions between neighboring phenanthroline rings.[28] The structure of DMPZ is given in Figure 1.

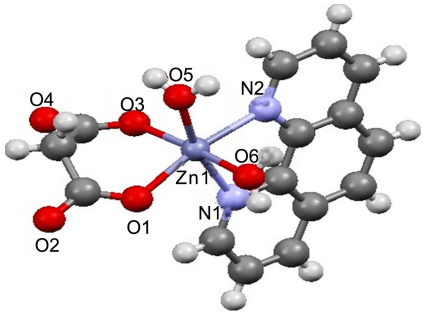

Figure 1. Molecular structure of DMPZ. In the structure, Zn1 is coordinated by N1 and N2 atoms of 1,10-phenanthroline, O5 and O6 atoms of water and O1 and O3 atoms of malonate dianion.

Results and Discussion

Optical Absorption Studies. Powder optical spectrum of VO(II)/DMPZ is recorded at 300 K and it is shown in Figure 2. It shows four bands at 30 395, 24 095, 17 730 and 11 649 cm^{-1}. First band is assigned as CT band and remaining three bands are due to d-d transitions. By comparison with the optical absorption spectra of other complexes containing VO(II), these bands are assigned to the transitions from ground state ^2B2g and those are, $^2B2g \rightarrow {}^2Eg$, $^2B2g \rightarrow {}^2B1g$, and $^2B2g \rightarrow {}^2A1g$ respectively,

$^2B2g \rightarrow {}^2Eg \rightarrow E1 = -3Ds + 5Dt$

$^2B2g \rightarrow {}^2B1g \rightarrow E2 = 10Dq$

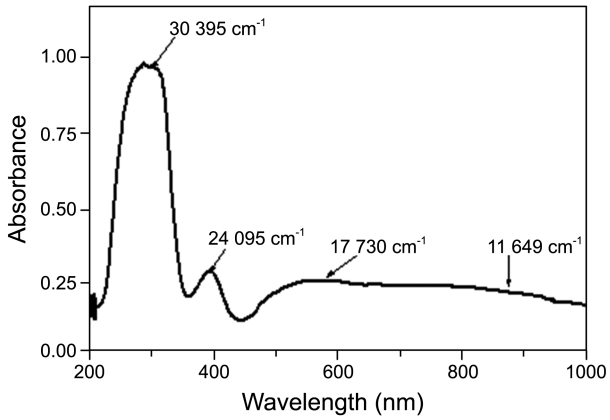

Figure 2. The Optical absorption spectrum of VO(II)/DMPZ.

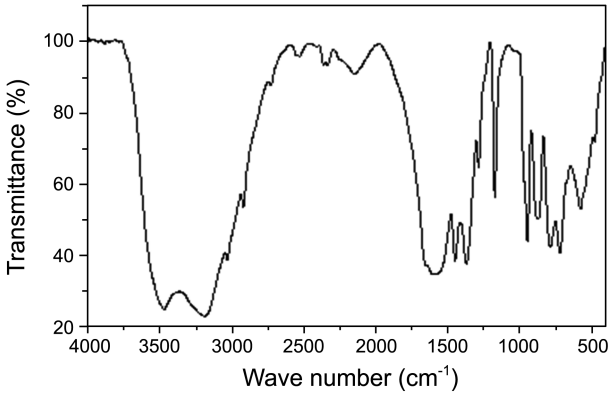

Figure 3. FT-IR Spectrum of VO(II)/DMPZ at RT.

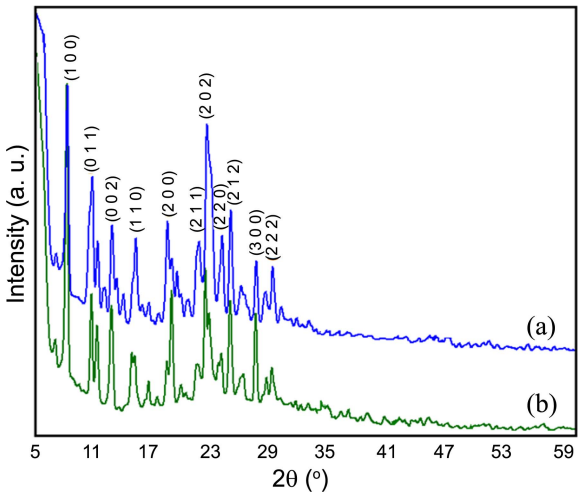

Figure 4. (a) Powder XRD pattern of VO(II) doped DMPZ and (b) pure DMPZ.

Table 1. The calculated lattice parameters of DMPZ and VO(II)/DMPZ from powder XRD, along with single crystal XRD of DMPZ[28]

Lattice parameters (nm) of from single crystal XRD	Lattice parameters (nm) calculated from powder XRD	
DMPZ	DMPZ	VO(II)doped DMPZ
a = 1.0336	a = 1.0572	a = 1.0570
b = 0.9666	b = 0.9779	b = 0.9775
c = 1.5474	c = 1.5750	c = 1.5769

$$^2B1g \rightarrow {}^2A1g \rightarrow E3 = 10Dq - 4Ds - 5Dt$$

Here, Dq is the octahedral crystal field parameter and Ds and Dt are the tetragonal crystal field parameters. The parameters evaluated from the above expressions are[29] Dq = 2409, Ds = –2573 and Dt = 786 cm^{-1}. These results indicate that the symmetry of vanadyl ion in the zinc host lattice is a distorted octahedron.

Infrared and Powder XRD Studies. The IR spectrum of VO(II)/DMPZ is recorded at room temperature and it is given in Figure 3. The carboxylate symmetrical stretching frequency is observed at 1572 cm^{-1} and the bands appeared at 3467 and 3183 cm^{-1} are assigned to O-H bending of water ligand. Three bands observed at 945, 787 and 787 cm^{-1} corresponds to bending modes of O-C-O bond. The band observed at 1450 is assigned to C=C stretching. The band observed at 1572 is assigned to carbonyl stretching.

The powder XRD patterns for undoped and VO(II) doped DMPZ were recorded. Figure 4(a) shows the powder XRD pattern for VO(II) doped DMPZ. From the patterns, the lattice parameters were calculated for undoped and doped complex and are given in Table 1, along with the single crystal data. These results indicate that the two complexes DMPZ and vanadyl doped DMPZ have identical lattice parameters. This observation further confirms that doping a low concentration of vanadyl impurity does not change the structure and hence lattice parameters of DMPZ.

Table 2. The spin Hamiltonian parameters obtained from the single crystal rotations of VO(II)/DMPZ using EPR-NMR program[31] and A in units of mT

Principal values				Direction cosines		
				a	b	c*
g matrix						
1.974	-0.002	-0.003	1.985	0.2104	0.8896	-0.4046
	1.971	-0.015	1.979	-0.9720	0.2344	0.0100
		1.950	1.943	0.1034	0.3912	0.9144
A matrix (mT)						
9.06	3.70	1.85	8.71	0.2073	0.9183	-0.3370
	7.80	3.60	6.41	0.9690	-0.1933	0.1480
		16.12	17.80	0.1276	-0.3699	0.9214

EPR Studies. Proper shaped crystals are selected for EPR rotation and it is mounted at the bottom of goniometer. Then it is placed inside a microwave cavity and single crystal rotations were made in three mutually orthogonal planes namely ab, bc* and ac* at 300K by passing the magnetic field, b is the crystallographic axis b, axis a is orthogonal to axis b in ab plane and axis c* is mutually perpendicular to both axes b and a. The EPR spectra of VO(II)/DMPZ single crystal exhibit eight hyperfine lines in all the three planes ab, ac*, bc* confirming the presence of only one type of impurity in the crystal even the unit cell contains four molecules. Typical EPR spectra of VO(II) doped DMPZ are given in Figures 5(a) and 5(b), when applied magnetic field (B) is parallel to two axes a and c* respectively. Vanadyl shows eight resonance lines, with equal intensity and spacing in all the three planes of rotation. It clearly indicates the absence of quadrupolar interaction. The spin Hamiltonian parameters are evaluated by using the EPR-NMR program,[30]

$$H = \Sigma [\beta (gi.Bi.Si) + Si.Ai.Ii], \quad (1)$$

i = x, y and z and x, y and z are the principle axes of g and A values. The other symbols are having their usual meanings. Inclusion of the nuclear quadrupolar and nuclear Zeeman

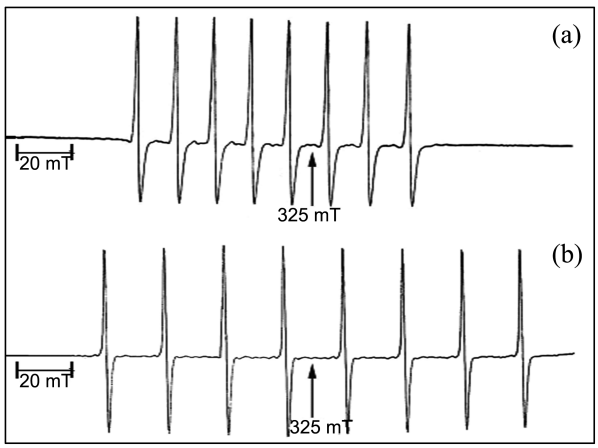

Figure 5. (a) Single crystal EPR spectrum of VO(II)/DMPZ, where the applied magnetic field (B) is parallel to axis a at 300 K, ν = 9.08436 GHz. (b) Single crystal EPR spectrum of VO(II)/DMPZ, where B is parallel to axids c* at 300K, ν = 9.08436 GHz.

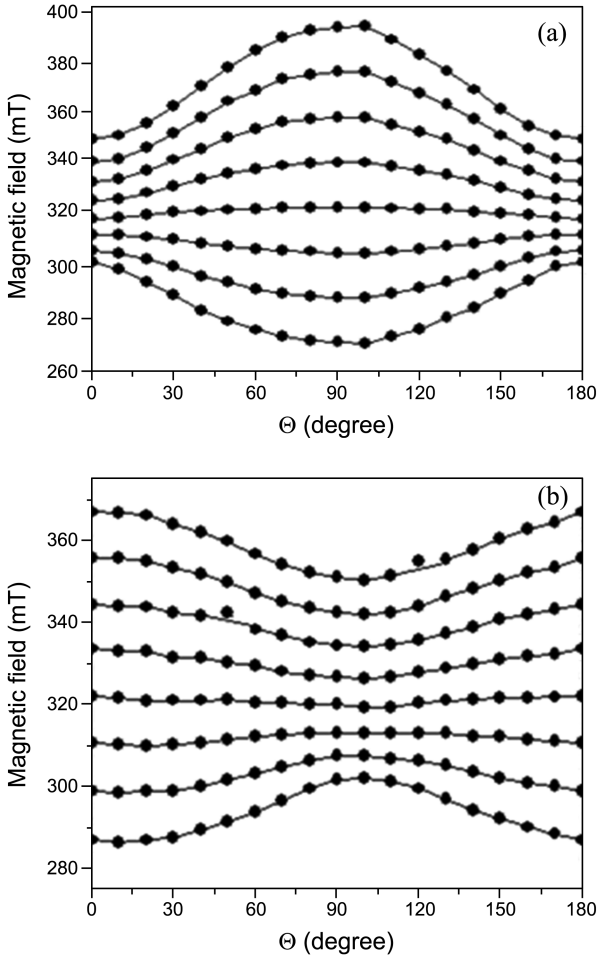

Figure 6. (a) Angular variation plot for VO(II)/DMPZ in ac* plane at 298 K, ν = 9.07578 GHz (b) Angular variation plot for VO(II)/DMPZ in ab plane at 298 K, ν = 9.08346 GHz (solid circles are experimental points and solid lines are theoretically calculated points).

interactions in the spin Hamiltonian during fitting experimental data using program EPR-NMR does not improve the fit or change the parameters (g and A). Hence, these parameters are not included in the final refinement. In addition, the intensity and separation of resonance lines also suggest minor contribution from nuclear quadrupolar interaction. The calculated spin Hamiltonian parameters are presented in Table 2.

The direction cosines of the principal values of g and A are nearly coincident. The eigen values of g and A indicate that the electrostatic field around the VO(II) ion is axial, even though deviation is noticed in hyperfine values. Using the parameters in Table 2, angular variation plots of all the three planes are simulated and are found to agree well with the experimental ones. The resultant isofrequency plots obtained for ac* and ab planes containing experimental and theoretical values are shown in Figures 6(a) and 6(b). A good concurrence is obtained indicating the accuracy of the spin Hamiltonian parameters. These spin Hamiltonian parameters are in agreement with other literature values. [23-27]

Generally, the direction cosines of the principal g/A values,

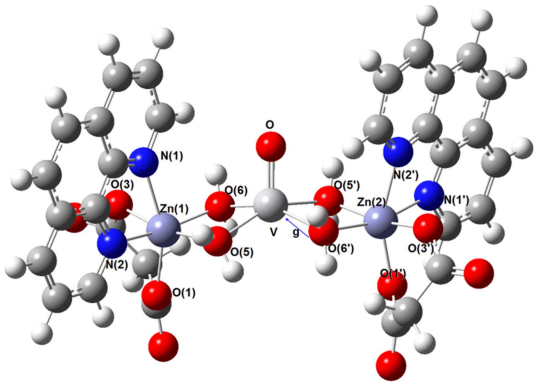

Figure 7. An Interstitial location giving distorted square pyramidal structure to vanadyl ion in the DMPZ lattice (see text for details). In this figure, blue atoms indicate Nitrogen atoms from 1,10-phenanthroline ring and red atoms indicate oxygen atoms from malonato anion and water. Also included is direction of principal g value, which is along V-O(6') direction.

obtained from EPR-NMR program are compared with metal -ligand bonds directions of the host lattice, to get information about the position of the dopant. From the crystal data of the host lattice,[28] the direction cosines of the various Zn-O and Zn-N bonds are calculated and it is given in the Table 3.

The direction cosines of various metal–ligand bonds are compared with that of g, A and it is found that none of them is matched, indicating the paramagnetic ion might have entered the lattice interstitially not substitutionally. In general, if the host ion is surrounded by six water molecules, VO(II) may occpy a substitution position in a distorted octahedral site because of the presence of strong vanadyl oxygen bond but in the present case, VO(II) impurity enters the lattice interstitially.

It is due to the strong coordination of zinc atom with 1,10-phenanthroline and malonic acid moiety and thus the breaking of the bond is very difficult. In addition, the impurity being the molecular ion, VO(II) cannot occupy neither octahedral nor polyhedral sites without removing any other bonds due to the presence of strong V=O bond. Hence, the paramagnetic impurity enters the lattice in an interstitial position is proved. EPR results suggesting paramagnetic impurity has entered interstitially, so a number of positions for vanadyl in the DMPZ lattice are assumed from XRD data of the host lattice. Procedure used for Cu(II) and VO(II) ion in diaqua(2,2'-bipyridine)malonatozinc(II) had been adopted here also.[24] The Cartesian coordinates for the zinc atoms, surrounding water, phenanthroline molecules and malonate anions in the unit cell can be calculated by making use of fractional coordinates and unit cell dimensions.[28] The exact interstitial arrangement of VO(II) in DMPZ is calculated out of all assumptions made and shown in Figure 7. It has been found that VO(II) ion bounded by four oxygen atoms: four of them namely O(5), O(5'), O(6) and O(6') are from water molecules connected to Zn(1) and Zn(2), with roughly represents a distorted square pyramidal geometry. The direction cosines of four V-O bonds are given in Table 3. The

Table 3. Direction cosines of Zn-O and Zn-N bonds in DMPZ lattice for site-I and site-II, along with the directions of interstitial site

M-L bond	Direction Cosines		
	a	b	c*
Site-I			
Zn(1) – N(1)	0.8132	0.3960	0.4262
Zn(1) – N(2)	0.4257	-0.7878	0.4452
Zn(1) – O(1)	-0.2823	0.8950	-0.3453
Zn(1) – O(3)	0.4290	-0.1765	-0.8859
Zn(1) – O(5)	-0.8221	-0.5238	-0.2231
Zn(1) – O(6)	-0.5344	0.2299	0.8134
Site-II			
Zn(2) – N(1')	-0.8133	-0.3961	-0.4262
Zn(2) – N(2')	-0.4257	0.7878	-0.4452
Zn(2) – O(1')	0.2823	-0.8950	0.3453
Zn(2) – O(3')	-0.4290	0.1765	0.8858
Zn(2) – O(5')	0.8218	0.5237	0.2244
Zn(2) – O(6')	0.5344	0.2299	0.8134
Interstitial location			
V – O(5)	-0.1946	0.8305	0.5219
V – O(5')	0.0774	0.5474	0.7421
V – O(6)	0.3026	0.9498	0.0790
V – O(6')	0.3949	0.9044	0.1202

Oxygen atoms labelled (1) and (3) represent malonato oxygens, whereas atoms (5) and (6) represent water oxygens. N(1) and N(2) represent 1,10-phenanthroline ligand nitrogens. For numbering of atoms, see Figure 6.

direction cosine of new location of V-O(6') bond matched with one of the direction cosines of the g matrix.

Polycrystalline Spectrum. Spin Hamiltonian parameters obtained from single crystal of VO(II)/DMPZ using EPR-NMR program has been confirmed by recording polycrystalline spectrum of VO(II)/DMPZ and it is shown in Figure 8. The powder EPR spectrum shows eight parallel and eight perpendicular lines and it suggests the axial nature of impurity. This is commonly being observed in most of the VO(II) systems. The g and A values which is calculated from powder spectrum are,

$$g_{\parallel} = 1.949,\ g_{\perp} = 1.996,\ A_{\parallel} = 19.5,\ A_{\perp} = 7.50\ \text{mT}$$

Using these parameters, the powder spectrum is simulated and it is given in the Figure 8. The simulated and the experimental spectra are found to be comparable. The powder spin Hamiltonian parameters are matched with the single crystal data. If the impurity is placed in an interstitial position of the lattice, the metal ligand bond lengths are infinitesimally large or small depending on the availability of coordination site.

Admixture Co-efficients. Admixture coefficients are also calculated from the spin Hamiltonian parameters. If C1, C2 and C3 are the admixture coefficients, where the ground state d_{xy} can mixes with $d_{x^2-y^2}$, d_{xy} and d_{yz}. These coefficients are related to g value by the relations,[31,32]

$$g_{\parallel} = 2(3C_1^2 - C_2^2 - 2C_3^2) \quad (2)$$

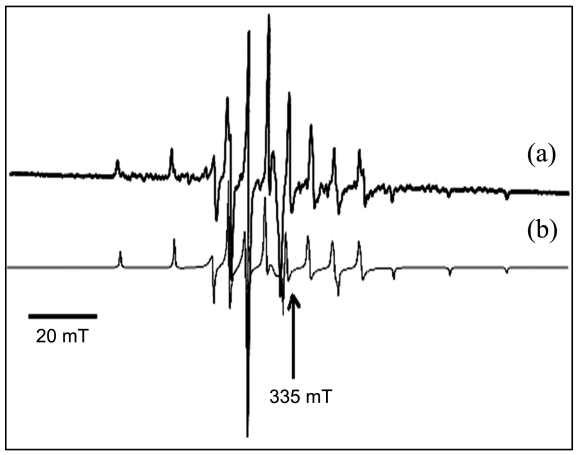

Figure 8. (a) Experimental Polycrystalline EPR spectrum of VO(II)/DMPZ (b) simulated EPR spectrum recorded at 300 K, ν = 9.39314 GHz.

$$g_{\perp} = 4C_1(C_2 - C_3) \quad (3)$$

and recalculated along with the normalization condition,

$$C_1^2 + C_2^2 + C_3^2 = 1 \quad (4)$$

Eqs. (2)-(4) can be solved iteratively for the admixture coefficients. The values of C_1, C_2, and C_3 thus evaluated are 0.7027, 0.7102, and 0.040, respectively. Two more parameters, *i.e.*, Fermi contact (κ) and dipolar interaction (P) are calculated from,

$$A_{\parallel} = P\,[-(4/7) - \kappa + (g_{\parallel} - g_e) + (3/7)\,(g_{\perp} - g_e)] \quad (5)$$

$$A_{\perp} = P\,[(2/7) - \kappa + (11/14)(g_{\perp} - g_e)] \quad (6)$$

Here, $P = g_e\beta_e\beta_n g_n\langle r^3\rangle$ and κ is a dimensionless constant describing the core s-polarization and represents the amount of unpaired electron density at the vanadium nucleus.

The values of P and κ are calculated from powder g and A values. In the present case, the P and κ values are -132×10^{-4} cm^{-1} and 0.85 respectively. These data are good concurrence with reported values.[33-38] The reduction of P value from the free ion (0.0017 cm^{-1}) gives the covalency of metal-ligand bond and for the present case it is 22%.

Conclusion

Single crystal EPR investigation of VO(II)/DMPZ is studied. During crystal rotation, eight line patterns are observed indicating single vanadyl site present in the host lattice. The g, A parameters and its direction cosines are calculated from EPR analysis. By comparing direction cosines acquired form EPR data with those calculated from crystal structure data, the vanadyl ion is occupied in an interstitial position due to strong coordination of malonic acid and phenanthroline ligand with zinc host lattice. Vanadyl ion is located in distorted square pyramidal geometry with four oxygen atoms of water molecules connected to two zinc atoms of host lattice. The isofrequency plots and powder EPR spectrum

are also simulated. The Fermi contact and dipolar interaction parameters are calculated, which gives an idea about the covalency of metal ligand bond. The optical absorption spectrum is helpful for the calculation of crystal field parameters, which reflects the symmetry of the dopant. FTIR and powder XRD data confirms the structure of host lattice and indicates no structural changes acquired during the incorporation of the paramagnetic impurity.

Acknowledgments. The publication cost of this paper was supported by the Korean Chemical Society.

References

1. Perez, C. R.; Martin, Y. R.; Molina, M. H.; Delgado, F. S.; Pasan, J.; Sanchiz, J.; Lloret, F.; Julve, M. *Polyhedron* **2003**, *22*, 2111.
2. Pasan, J.; Delgado, F. S.; Martin, Y. R.; Molina, M. H.; Perez, C. R.; Sanchiz, J.; Lloret, F.; Julve, M. *Polyhedron* **2003**, *22*, 2143.
3. Levstein, P. R.; Calvo, R. *Inorg. Chem.* **1990**, *29*, 1581.
4. Colacio, E.; Dominguez-Vera, J. M.; Costes, J. P.; Kivekas, R.; Laurent, J. P.; Ruiz, J.; Sundberg, M. *Inorg. Chem.* **1992**, *31*, 774.
5. Colacio, E.; Dominguez Vera, J. M.; Kivekas, R.; Moreno, J. M.; Romerosa, A.; Ruiz, J. *Inorg. Chim. Acta* **1993**, *212*, 115.
6. Gardner, G. B.; Venkataraman, D.; Moore, J. S.; Moore, S. *Nature* **1995**, *374*, 792.
7. Chattopadhya, D.; Chttopadhyay, S. K.; Lowe, P. R.; Schwalbe, C. H.; Mazumder, S. K.; Rana, A.; Ghosh, S. *J. Chem. Soc. Dalton Trans*. **1993**, *41*, 913.
8. Bruce, S. *J. Drugs Dermatol*. **2008**, *7*, 17.
9. Hoffmann, S. K.; Goslar, J.; Tadyszak, K. *J. Magn. Reson.* **2010**, *205*, 293.
10. Pandey, S.; Kripal, R. *J. Magn. Reson.* **2011**, *209*, 220.
11. Yerli, Y.; Zerentürk, A.; Özdoan, K. *Spectrochim. Acta* **2007**, *A68*, 147.
12. Sigel, H. *Metal Ions in Biological Systems*, Marcel Dekker Inc.: New York, 1974.
13. Kripal, R.; Maurya, M.; Govind, H. *Physica B* **2007**, *392*, 281.
14. Velavan, K.; Venkatesan, R.; Rao, P. S. *Spectrochim. Acta* **2005**, *A62*, 153.
15. Deepa, S.; Velavan, K.; Sougandi, I.; Venkatesan, R.; Rao, P. S. *Spectrochim. Acta* **2005**, *A61*, 2482.
16. Karabulut, B.; Tufan, A. *Spectrochim. Acta* **2006**, *A65*, 742.
17. Viswanath, A. K. *J. Chem. Phys*. **1977**, *67*, 3744.
18. Maurya, B. P.; Punnoose, A.; Umar, M.; Singh, R. J. *Solid State Commun.* **1994**, *89*, 59.
19. Angeli Mary, P. A.; Dhanuskodi, S. *Spectrochim. Acta* **2001**, *A57*, 2345.
20. Kripal, R.; Singh, P. *J. Mag. Magn. Materials* **2006**, *307*, 308.
21. Shiyamala, C.; Mithira, S.; Natarajan, B.; Ravikumar, R. V. S. S. N.; Rao, P. S. *Phys. Scr.* **2006**, *74*, 549.
22. Natarajan, B.; Mithira, S.; Deepa, S.; Ravikumar, R. V. S. S. N.; Rao, P. S. *Radiat. Eff. Defects. Solids* **2006**, *161*, 177.
23. Natarajan, B.; Mithira, S.; Deepa, S.; Rao, P. S. *J. Phys. Chem. Solids* **2007**, *68*, 1995.
24. Parthipan, K.; Hema, R.; Rao, P. S. *J. Mol. Struct.* **2011**, *992*, 59.
25. Arun Prasad Lingam, K.; Mithira, S.; Rao, P. S. *Appl. Magn. Reson.* **2010**, *382*, 295.
26. Natarajan, B.; Mithra, S.; Deepa, S.; Rao, P. S.; Ravikumar, R. V. S. S. N. *Radiat. Eff. Defects Solids* **2006**, *161*, 177.
27. Tapramaz, R.; Karabulut, B.; Koksal, F. *J. Phys. Chem. Solids* **2000**, *611*, 1367.
28. Fu, X. C.; Li, M. T.; Wang, C. G.; Wang, X. Y. *Acta Cryst.* **2006**, *C62*, m13-m16.
29. Ballhausen, C. J.; Gray, H. B. *Inorg. Chem.* **1962**, *1*, 111.
30. Clark, F.; Dickson, R. S.; Fulton, D. B.; Isoya, J.; Lent, A.; McGavin, D. G.; Mombourquette, M. J.; Nuttal, R. H. D.; Rao, P. S.; Rinnerberg, H.; Tennat, W. C.; Weil, J. A. *EPR-NMR Program*, University of Saskatchewan, Saskatoon, Canada, 1996.
31. Jain, V. K. *Phys. Stat. Sol.* **1980**, *B97*, 337.
32. Dhanuskodi, S.; Angeli Mary, P. A.; Vasantha, K. *Spectrochim. Acta* **2003**, *A59*, 927.
33. Kivelson, D.; Lee, S. K. *J. Chem. Phys*. **1964**, *41*, 1896.
34. Vasantha, K.; Angeli Mary, P. A.; Dhanuskodi, S. *Spectrochim. Acta* **2002**, *A58*, 311.
35. Gopal, N. O.; Narasimhulu, K. V.; Rao, J. L. *Physica* **2001**, *B307*, 117.
36. Biyik, R. *Physica* **2009**, *B392*, 3483.
37. Kripal, R.; Maurya, M. *Solid State Commun.* **2010**, *150*, 95.
38. Yerbasi, Z.; Karabulut, A.; Karabulut, B. *Spectrochim. Acta* **2011**, *A79*, 1304.